J. Fluid Mech. (2006), *vol.* 547, *pp.* 149–173.
doi:10.1017/S0022112005007652 Printed in the United Kingdom

Experimental investigation of a bioartificial capsule flowing in a narrow tube

By FRÉDÉRIC RISSO†, FABIENNE COLLÉ-PAILLOT AND MOKHTAR ZAGZOULE

Institut de Mécanique des Fluides de Toulouse, UMR 5502 CNRS-INP-UPS, Allée C. Soula, 31400, Toulouse, France

(Received 28 February 2005 and in revised form 7 July 2005)

This work is an experimental study of the motion and deformation of a bioartificial capsule flowing in a tube of 4 mm diameter. The capsules, initially designed for medical applications, are droplets of salt water surrounded by a thin polymeric membrane. They are immersed in a very viscous Newtonian silicone oil that flows through a tube in the Stokes regime. The properties of the capsules were carefully determined. Two previous experimental papers were devoted to their characterization by osmotic swelling and compression between two plates. The present work also provides a series of tests that allows an accurate definition of the experimental model under investigation. The capsules are buoyant and initially quasi-spherical. Nevertheless, buoyancy and small departures from sphericity are shown to have no significant effects, provided the flowing velocity is large enough for the viscous stress to become predominant. The capsules are also initially slightly over-inflated, but there is no mass transfer through the membrane during the present experiments. Their volume therefore remains constant. The membrane can be described as an elastic two-dimensional material, the elastic moduli of which are independent of the deformation. Far from the tube ends, the capsule reaches a steady state that depends on two parameters: the capillary number, Ca; and the ratio of the radius of the capsule to that of the tube, a/R. The capillary number, which compares the hydrodynamic stresses to the elastic tensions in the membrane, was varied between 0 and 0.125. The radius ratio, which measures the magnitude of the confinement, was varied from 0.75 to 0.95. In the range investigated, the membrane material always remains in the elastic domain. At fixed a/R, the capsule is stretched in the axial direction when Ca is increased. The process of deformation involves two main stages. At small to moderate Ca, the lateral dimension of the capsule decreases whereas its axial length increases. The capsule is rounded at both ends, but the curvature of its rear decreases as Ca increases. At large Ca, the rear buckles inward. Then, the negative rear curvature goes on decreasing whereas the lateral dimension of the capsule reaches a constant value. On the other hand, increasing a/R promotes the deformation: the process remains qualitatively the same, but the different stages are attained for smaller values of Ca. Comparisons with available numerical simulations show that the results are strongly dependent on the properties of the capsules.

† Author to whom correspondence should be addressed. risso@imft.fr.

1. Introduction

There are many situations that require the transport and delivery of a given quantity of an active substance at a precise time and location. Because it is either fragile and must be protected or toxic and must not be released into the environment, the substance has to be isolated. The living cell constitutes a solution to this problem. Based on the same principle, artificial capsules are increasingly used in various domains such as medicine, cosmetics and agriculture. Like living cells, artificial capsules are made of a deformable membrane that separates the inner fluid, which contains the active substances, from the outer one. (Hereinafter, the word capsule will refer to both living cells and artificial capsules.) There are two ways of ensuring the release of encapsulated substances, the membrane may either rupture or be specifically permeable to certain molecules. The study of capsules involves different scientific fields. Physics, biology and chemistry are, of course, crucial for the determination of the physical properties of the membrane as well as their biological compatibility. In particular, many works have been devoted to the mechanical properties of either living cells (see Mohandas & Evans 1994; Smith *et al.* 2000 and references therein) or synthetic capsules (Edwards-Lévy & Lévy 1999; Disher *et al.* 2002 and references therein). On the other hand, coupled with membrane mechanics, the fluid dynamics control the deformation and the motion of the capsules.

Capsules often have to flow in small vessels in order to bring the active substance up to the location where it has to be released. In these situations, the capsule experiences strong deformation resulting from complex fluid–structure interactions. Especially motivated by blood micro-circulation (see Skalak, Özkaya & Skalak 1989 and references therein), numerous works have been devoted to the study of capsules in various flows. On the one hand, theoretical works assume a particular constitutive law for the membrane, a given initial shape for the capsule and a specific model for the mass transfer between the inner and outer media. Studies of the deformation of a capsule in different basic unbounded shear flows were initiated by Barthès-Biesel (1980) who calculated the small deformations of a capsule suspended in a simple shear flow. Studies of capsules flowing in narrow channels were first addressed by using lubrication theory (see Secomb *et al.* 1986). Now these situations can be solved numerically by using boundary integral methods. For unbounded flow, see Ramanujan & Pozrikidis (1998), Diaz, Pelekasis & Barthès-Biesel (2000), Pozrikidis (2001), Lac *et al.* (2004) and references therein. For a capsule in a narrow tube, simulations have been performed by Quéguiner & Barthès-Biesel (1997), Diaz (2001) and Diaz & Barthès-Biesel (2002).

On the other hand, if we except qualitative descriptions of red blood cells flowing in micro-vessels, experimental investigations of a capsule immersed in a flow are rare. As far as we know, the most advanced study was by Chang & Olbricht (1993*a*, *b*). They studied the deformation of a synthetic capsule in extensional and simple shear flows. The elastic moduli of the membrane were obtained from comparisons with small-deformation theory and independent compression experiments. At large strain rate, they reported plastic deformation and even membrane rupture. They also observed effects that suggested that the membrane was viscoelastic. Concerning capsules flowing in narrow tubes, we are aware of only two experimental investigations: the pioneering work of Lee & Fung (1969) who considered biconcave thin-walled rubber cells; and the investigation of lipid vesicles by Vitkova, Mader & Podgorski (2004). These two investigations provided interesting descriptions, but cannot be compared with theoretical predictions since the values of the elastic moduli of the membranes are not provided by the authors.

The present work is a new experimental investigation of a bioartificial capsule flowing in a narrow tube. The diameter of the capsules, which were initially designed by Lévy & Edwards-Lévy (1996) for medical applications, is 3–4 mm. Such a large size simplifies manipulations and allows the use of the video acquisition and processing techniques that we have developed and improved in the context of bubbly flows over fifteen years. In addition, it makes possible a better characterization of the capsules properties. However, most of the applications involve capsules of a few micrometres. With the aim that the results should also be relevant for micro-capsules, we selected capsules with a very thin membrane, which could be modelled as a two-dimensional material, and chose an external fluid that ensured that both buoyancy and inertial effects were negligible. Since the results necessarily depend on capsule properties, we took great care in their characterization. In a previous work devoted to the study of the mass transfer through the membrane (Sherwood *et al.* 2003), the initial pressure of the inner liquid was determined. This allows the determination of the reference state of the capsule in absence of flow: even if the capsule takes a spherical shape, the membrane experiences an initial extension of about 5 %. Risso & Carin (2004) determined the mechanical law of the membrane from compression experiments: the membrane is purely elastic with elastic moduli independent of the deformation. The present work thus provides an accurate description of the behaviour of capsules of reasonably well-known properties. The capsules are presented in § 2 and the experimental facility and instrumentation are described in § 3. In § 4, we test the influence of the small imperfections of the experimental model (slight non-sphericity, small buoyancy effect, uncertainty in the elastic moduli) and show that the results depend on two control parameters: the capsule-to-tube radius ratio, a/R, and the capillary number, $Ca = \eta_{ext}U/K$, which compares the hydrodynamics viscous stress $\eta_{ext}U/a$ to the elastic one K/a (η_{ext} and U are the viscosity and bulk velocity of the outer-fluid, K is a membrane elastic modulus). The main results are presented in § 5. They focus on the steady state reached by the capsule far from the tube ends for a/R in the range $0.75 - 0.95$ and for Ca up to 0.125. In § 6, the present results are compared with those available in the literature and the roles of membrane rheology and initial inflation are discussed.

2. The capsules

The membrane of the capsules is made of covalently linked human serum albumin (HSA) and alginate (Lévy & Edwards-Lévy 1996; Edwards-Lévy & Lévy 1999). Calcium-alginate gel beads coated with HSA-alginate membranes were originally designed for medical applications such as hepatocyte encapsulation for bioartificial liver (Joly *et al.* 1997) or encapsulation of genetically modified cells for AIDS treatment (Shinya *et al.* 1999). The present capsules were first prepared according to the procedure described by Edwards-Lévy & Lévy (1999). Then, the gel core of the coated beads was re-liquified by sodium citrate in order to obtain capsules with a liquid core surrounded by a membrane of cross-linked HSA and alginate. Finally, a small amount of basilen blue was added to the inner liquid in order to make the capsules easier to detect by optical means. These capsules are thus constituted of a thin elastic membrane that enclosed an inner liquid, which is essentially coloured salt water. Initially, the outer liquid was a $9\,\mathrm{g\,l^{-1}}$ aqueous solution of sodium chloride. The properties of the capsules differ slightly from one to another. They are almost spherical with radii ranging between 1.4 and 1.9 mm. The membrane thickness, h, was measured by Carin *et al.* (2003), they are of either 20 or 30 μm depending on

a small change in the fabrication process. Two previous works were devoted to the determination of the specific properties of the capsules used here. First, Risso & Carin (2004) investigated the mechanical properties of the membranes from compression experiments. The capsule was squeezed between two plates and the relationship between the compression force and the capsule deformation was recorded. For capsules with such a thin membrane, it was shown that the membrane could be described as a two-dimensional material with negligible membrane stiffness. Evans & Skalak (1980) established the general expression of the mechanical constitutive law for an isotropic homogeneous purely elastic two-dimensional material with negligible bending stiffness. Noting λ_1 and λ_2 as the principal extension ratios, the deformation is fully characterized by the two independent invariants $\alpha = \lambda_1\lambda_2 - 1$ and $\beta = (\lambda_1/\lambda_2 + \lambda_2/\lambda_1)/2 - 1$. In the principal axes, the first component of the tension is

$$T_1 = K\,\alpha + \mu\frac{\lambda_1^2 - \lambda_2^2}{2\lambda_1^2\lambda_2^2}, \tag{2.1}$$

the second component is obtained by exchanging subscripts 1 and 2. The area dilation modulus K and the area shear modulus μ are functions of the two invariants α and β. These two functions, $K(\alpha, \beta)$ and $\mu(\alpha, \beta)$, define the mechanical constitutive law of the material. It is worth noting that (2.1) can be used to model either a membrane consisting of a few layers of molecules or a thin sheet of a three-dimensional material. In this latter case, the thickness h of the sheet is a function of the deformation. In the limit of small deformations, $e_1 = 1/2(\lambda_1^2 - 1) \ll 1$ and $e_2 = 1/2(\lambda_2^2 - 1) \ll 1$, equation (2.1) becomes

$$T_1 = K_0(e_1 + e_2) + \mu_0(e_1 - e_2), \tag{2.2}$$

where K_0 and μ_0 are the limits of the functions K and μ when α and β tend towards zero. Equation (2.2) is the two-dimensional Hooke's law, in which the Young's modulus is $E = 4K_0\mu_0/(K_0 + \mu_0)$ and the Poisson ratio $\nu = (K_0 - \mu_0)/(K_0 + \mu_0)$. When (2.1) is used to described a thin sheet of a three-dimensional material, the moduli K_0 and μ_0 of the two-dimensional material can be derived from the Young's modulus, E_{3D}, and the Poisson ratio, ν_{3D}, of the three-dimensional material. By making the membrane thickness h tending towards zero, it is found that $2K_0 = hE_{3D}/(1 - \nu_{3D})$ and $2\mu_0 = hE_{3D}/(1 + \nu_{3D})$. When ν_{3D} varies from 0 to 1/2, μ_0/K_0 varies from 1 to 1/3. Any two-dimensional material with μ_0/K_0 in the range 1/3–1 can thus be considered as the limit of a homogeneous three-dimensional material of vanishing thickness.

The simplest constitutive law, hereinafter denoted ES, is obtained by considering that the two elastic moduli are independent of the deformation, $K = K_0$ and $\mu = \mu_0$. Even if it has more solid physical bases, the (ES) law is, for historical reasons, not as well known as another model (STZC) proposed by Skalak *et al.* (1973) for the description of the red blood cell:

$$T_1 = G^{STZC}\left(\frac{\lambda_1}{\lambda_2}\left(\lambda_1^2 - 1\right) + C^{STZC}\lambda_1\lambda_2\left(\lambda_1^2\lambda_2^2 - 1\right)\right). \tag{2.3}$$

The corresponding expressions of K and μ are complex and their limits in small deformations are $K_0 = G^{STZC}(1 + 2C^{STZC})$ and $\mu_0 = G^{STZC}$. On the other hand, the two-dimensional Mooney–Rivlin law (MR), which has been derived by considering an infinite thin sheet of incompressible elastomer, is commonly used,

$$T_1 = \frac{G^{MR}}{\lambda_1\lambda_2}\left(\lambda_1^2 - \frac{1}{\lambda_1^2\lambda_2^2}\right)\left(1 - \Psi' + \lambda_2^2\Psi'\right). \tag{2.4}$$

G^{MR} is a surface elastic modulus and Ψ' a non-dimensional parameter ranging from 0 to 1. The expressions of K and μ are again very complex, their limits in small deformations are $K_0 = 3G^{MR}$ and $\mu_0 = G^{MR}$.

Risso & Carin (2004) compressed capsules of different ages, from fresh capsules to capsules that have been conserved in their original aqueous solution for more than one year. Concurrently, they performed numerical simulations of the same problem by assuming a given constitutive law: ES (constant elastic moduli), MR and STZC models were tested. Only the ES model provided a good agreement with the measurements. Assuming that the elastic moduli were independent of the deformation was thus a good approximation in the range of deformation investigated ($\alpha \leqslant 1.5$). That was true for all capsules. From the point of view of mechanics, the only visible effect of the ageing process was to decrease the values of the elastic moduli. Because the area dilation plays the major role in compression experiments, it was possible to measure the area dilation modulus K independently of both the values of the shear modulus and that of a possible small bending modulus. (This latter, even very small, cannot be zero.) The value of K was thus obtained for each capsule with fairly good accuracy ($\pm 5\,\%$). On the other hand, it could be concluded only that the shear modulus ranged between $K/3$ and K, which is consistent with a thin sheet of a homogeneous three-dimensional material. For the present experiments, we selected 28 capsules of different ages and thicknesses from about two hundred available capsules. Our purpose was to use the widest possible ranges of elastic modulus and capsule size. We selected from visual inspection those which have a homogeneous membrane and the most spherical shape. To characterize the sphericity, we introduced the ratio $S = L_{min}/L_{max}$ between the maximal and minimal axes of the capsule (see figure 1). For the selected capsules, S ranged between 0.86 and 0.97 with an average of 0.94 and a standard deviation of 0.03. Nine of these capsules were tested in the compression apparatus and their area dilation modulus K was determined following the procedure described in Risso & Carin (2004). For the others, the modulus K was determined by comparing their stationary shapes within the narrow tube with the shapes of the capsules of known modulus (see § 3). The characteristics of all the capsules used in the present flow experiments are given in table 1.

Sherwood *et al.* (2003) studied the isotropic inflation or deflation of a capsule which was immersed in a sodium chloride aqueous solutions of various concentrations. The volume of the capsule was able to change because both salt and water can pass through the membrane. The volume of the capsule was shown to correspond to a Donnan equilibrium where the inner pressure is larger than the outer pressure because of the presence of a minute amount of polyelectrolyte molecules that were trapped inside the capsule. The relationship between the isotropic membrane extension, $\lambda_i = (1+\alpha)^{0.5}$, and the concentration C of the outer solution was derived: λ_i is a decreasing function of C which starts with a very large value for $C = 0$ and tends asymptotically towards unity as C tends towards infinity. That means that the capsules are always over-inflated ($\lambda_i \geqslant 1$), but relax towards their natural volume ($\lambda_i = 1$) when the concentration is increased. In the initial $0.9\,\mathrm{g\,l^{-1}}$ sodium chloride solution, λ_i was in the range 1.04–1.05. The continuous phase used in the present experiment was not salt water but silicone oil Rhodorsil 47V1000. The capsules were carefully extracted from the original solution and immersed in the silicone oil. The oil molecules are too large to pass through the membrane, but water can. A few test capsules were observed during a long time after they had been moved into the oil. We observed that the water indeed passed through the membrane and that the capsules shrank very slowly. It took six weeks to empty the capsules completely. As the present experiments never exceeded

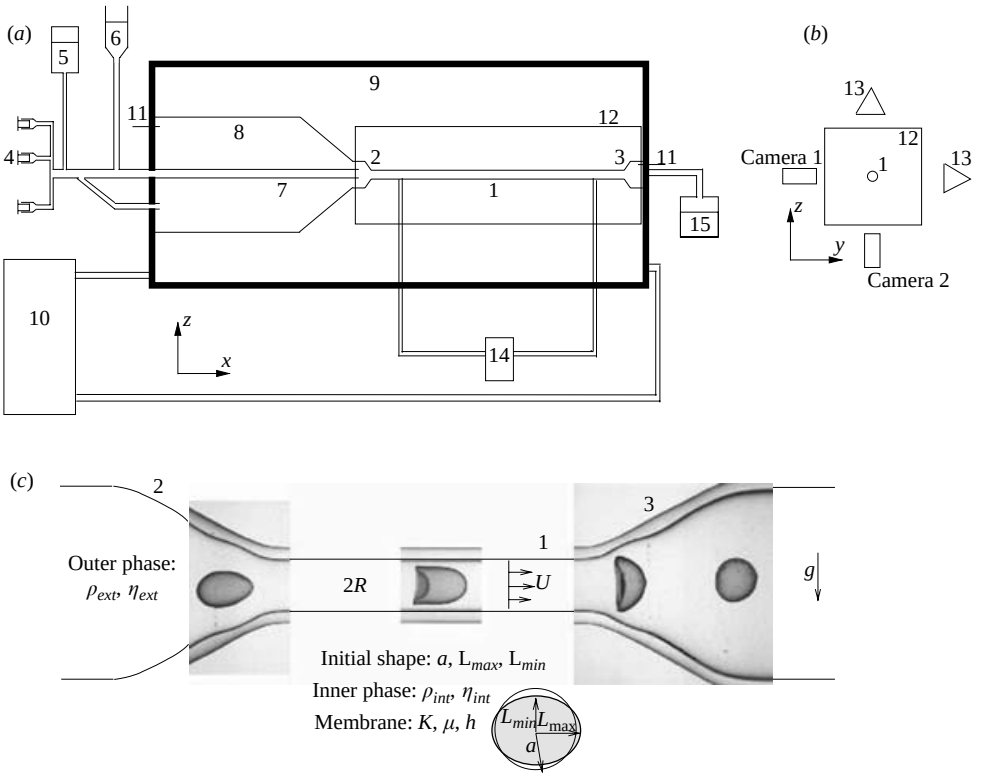

FIGURE 1. Schematic of the experimental facility (not to scale): 1. test section; 2. converging section; 3. diverging section; 4. infusion-syringe pumps; 5. oil reservoir; 6. capsule inlet; 7. supply tube; 8. oil reservoir; 9. water bath; 10. cryostat; 11. thermocouples; 12. optical box; 13. lights; 14. differential pressure transducer; 15. exit reservoir.

6 h for a given capsule, the capsule volume had no time to change and remained equal to its initial value in the original sodium chloride solution. The capsule volume was also measured before, during and after the flow of a capsule inside the tube. The measured variations were indifferently negative or positive and always less than the experimental error ($\pm 2\,\%$).

3. Experimental facility and instrumentation

The experimental set-up is depicted in figure 1. The test section, 1, consists of a horizontal glass tube with an inner radius $R = 2$ mm and 220 mm length. A converging section, 2, precedes the test section and a diverging section, 3, follows it, ensuring smooth entering and exit of the capsule. The suspending fluid is Silicone oil Rhodorsil 47V1000 which is a Newtonian fluid with a density $\rho_{ext} = 970\,\mathrm{kg\,m^{-3}}$ and a viscosity $\eta_{ext} = 1.02$ Pa s at $21.7\,^{\circ}$C. It is supplied by means of three infusion-syringe pumps, 4, that provide a constant flow-rate and allow the bulk velocity to vary from 1 to $34\,\mathrm{mm\,s^{-1}}$. The syringes, which have a content of 50 ml each, are first filled from the reservoir, 5. A capsule is introduced by the capsule inlet, 6, while the fluid is at rest. Then, the pumps are switched on and both the fluid and the capsule flow in a supplying tube, 7, which is immersed in a oil reservoir, 8, of 1.2 l volume. The whole facility is located in an air-conditioned laboratory ($20 \pm 1.5\,^{\circ}$C). Moreover, the supply

Capsule	h (μm)	a/R	K (N m^{-1})	S
C1	30	0.78	1.7*	0.94
C2	30	0.81	1.8	0.97
C3	30	0.94	1.7*	0.93
C4	30	0.74	1.8	0.93
C5	30	0.80	1.8	0.95
C6	30	0.94	1.7	0.96
C7	20	0.78	1.0	0.97
C8	20	0.81	1.1	0.93
C9	20	0.77	0.95*	0.97
C10	20	0.79	1.0*	0.95
C11	30	0.76	0.55	0.92
C12	30	0.87	0.65	0.87
C13	30	0.77	0.55	0.97
C14	30	0.78	0.77*	0.96
C15	30	0.83	0.55*	0.91
C16	30	0.80	0.26	0.95
C17	30	0.81	0.26	0.96
C18	30	0.83	0.30*	0.93
C19	30	0.85	0.26	0.93
C20	30	0.82	0.32*	0.93
C21	30	0.84	0.40*	0.93
C22	30	0.75	0.80	0.88
C23	30	0.78	0.85	0.86
C24	30	0.79	0.75	0.93
C25	30	0.80	0.80	0.94
C26	30	0.80	0.80	0.94
C27	30	0.87	0.80	0.95
C28	30	0.78	1.30	0.97

TABLE 1. Characteristics of the capsules: membrane thickness, h; capsule radius relative to that of the tube, a/R (± 0.025); membrane area dilation elastic modulus K ($\pm 5\,\%$), values marked with a star were determined from compression experiment (Risso & Carin 2004), others were obtained from the present experiments (see § 4); spericity ratio, S.

tube, 7, the oil reservoir, 8, and the test section, 1, are immersed in a large water bath, 9, ($520 \times 180 \times 180\,\mathrm{mm}^3$), the temperature of which is controlled by means of a cryostat, 10. While the capsule travels through the stainless steel tube, 7, the flow has time to reach a steady sate and the temperatures of both the oil and the capsule have time to evolve from the laboratory temperature up to the temperature of the test section. All the experiments are thus conducted at the same temperature ($21.7 \pm 0.1\,^{\circ}\mathrm{C}$) which is continuously monitored by means of thermocouples, 11.

The pressure drop over the cross-section is measured by a differential pressure transducer. Preliminary tests have consisted in measuring the relationship between the pressure drop and the bulk velocity for six different temperatures ranging from 16 to 26 °C. The results have been compared to the Poiseuille law, the value of the oil viscosity being determined independently for all tested temperatures by means of a cone-plane rheometer. The discrepancy between the present measurement of U and the prediction of the Poiseuille law was small; it is maximal for very low flow rate ($\pm 2.5\,\%$ at $\mathrm{U} = 1\,\mathrm{mm\,s}^{-1}$), but decreases quickly when U is increased ($\pm 0.2\,\%$ at $U = 34\,\mathrm{mm\,s}^{-1}$). Note that the additional pressure drop caused by the passage of a capsule in the tube was negligible compared to the linear pressure drop. This ensured that the flow rate did not change during the entry or the exit of a capsule.

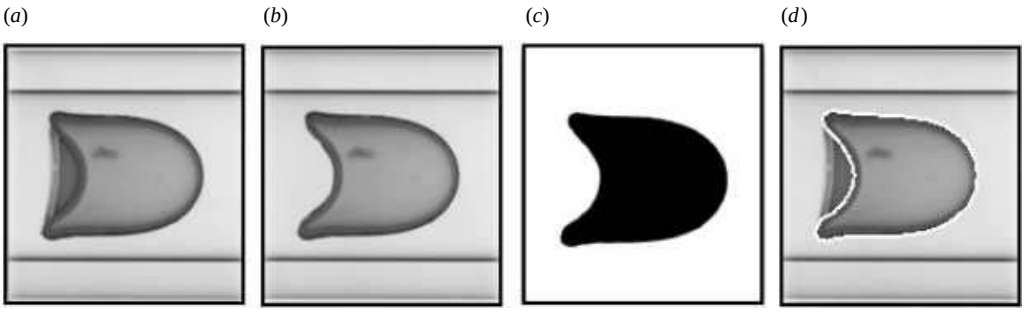

FIGURE 2. Contour detection: (*a*) initial picture, (*b*) manual erasing, (*c*) capsule detection, (*d*) comparison between detected contour and initial picture.

Unfortunately, this also implied that the additional pressure drop was under the range of the pressure transducer, 14, and could not be measured. Owing to the limitations of our instrumentation, the present work will not present results concerning this quantity.

Glass windows are located on the four lateral sides of the water bath, 9, allowing full optical access to the test section. An optical box, 12, made of glass and filled with silicone oil surrounds the test section to minimize optical distortion due to the curved surface of the tube. Two CCD cameras (Sony XC8500 with 782×582 pixels), equipped with lenses of 60 mm focal length, are used to film the capsule as it flows inside the test section. Since the lights, 13, are facing the cameras, the pictures show the capsule shadows (see figure 2). We thus obtain pictures of the projection of the capsule in the vertical plane (camera 1) and in a horizontal plane (camera 2). Data acquisition is ensured by the use of two computers. The first one triggers the two cameras and stores the digital pictures. The second records the temperatures provided by the thermocouples, 11, and the pressure drop provided by the pressure transducer, 14. The frequency of acquisition f is varied between 5 and 20 Hz depending on the liquid flow rate. In each case, the exposure time is 0.1 ms, which is short enough to freeze the capsule. Several successive tests are performed with the same capsule. In a first series, the two perpendicular cameras are located at the same axial position x. Simultaneous horizontal and vertical views of the capsule are taken in order to check the axisymmetry (see § 4). A second series is carried out by setting the two cameras at different axial locations. This allows us to check that the flow of the capsule has reached a steady state. For each capsule, the whole range of flow rates was tested ($1 \leqslant U \leqslant 34\,\mathrm{mm\,s^{-1}}$). The successive flow rates are tested in increasing order, starting from $U = 0$ in order to take a picture of the capsule at rest. Between each test at constant velocity U, the flow is reversed for the capsule to come back in the supplying tube and be ready for the next test. Several tests of reproducibility were also carried out in order to ensure that the capsule membrane remained in the elastic domain.

The capsule contour is detected afterwards by digital video processing in order to determine the capsule shape and velocity. Before each test, two reference images have been recorded: the background image in the absence of any capsules; and the calibration image in the presence of a spherical steel sphere of known size. The algorithm for contour detection involves five steps. We start with a raw image in 256 grey levels (figure 2*a*). Two different situations must be distinguished. Whenever the capsule shape exhibits a concave part, there are hidden parts on the shadowgraph. In this case, the first step consists in erasing manually the corresponding part of

the picture (figure 2*b*). If the capsule is convex, we go directly to the second step which is the subtraction by the background image. During the third step, the method of minimum variance is used to threshold the image. The fourth step is the image binarization, all pixels which have a grey level less than the threshold are set black, the others are set white (figure 2*c*). In the fifth step, the frontier between the black and white regions is detected. The superimposition of the detected contour on the raw image confirms that the method is reliable (figure 2*d*). The spatial resolution is given by the pixel size, which is 0.011 mm. Concurrently, the detection of the tube boundary was obtained with a similar algorithm, but another threshold. This fixes the accuracy on the capsule position and on the different dimensions that will be used to characterize the capsule shape (see § 5). The capsule velocity V is determined from the displacement of the capsule front between two successive images. Since the uncertainty on the time is negligible, the uncertainty on the capsule velocity is equal to the uncertainty on the detection of the capsule contour divided by the sampling time $1/f$. We therefore obtain an accuracy that is better for low sampling rates. We obtain finally that the uncertainty on V increases from $\pm 0.025\,\mathrm{mm\,s^{-1}}$ for $U = 1\,\mathrm{mm\,s^{-1}}$ up to $\pm 0.10\,\mathrm{mm\,s^{-1}}$ for $U = 34\,\mathrm{mm\,s^{-1}}$.

4. Problem statement and validation of the experimental model

Our objective is to study the steady state of a capsule made of an initially spherical drop of a Newtonian fluid surrounded by an impermeable elastic membrane of negligible thickness immersed in a Newtonian fluid that flows in a narrow tube in the absence of inertia and buoyancy. This ideal situation depends on the characteristics of the outer flow and on those of the capsule. The former are the density ρ_{ext} and viscosity η_{ext} of the outer fluid, the tube radius R and the bulk velocity U; the latter are the density ρ_{int} and viscosity η_{int} of the inner fluid, the capsule radius at rest and the two elastic moduli of the membrane, K and μ. The ideal problem hence depends on three dimensionless groups: the capillary number, $Ca = \eta_{ext}U/K$, which compares viscous and elastic forces; the capsule-to-tube radius ratio, a/R, which measures the geometrical confinement; and the ratio of the elastic moduli, K/μ, which characterizes the membrane rheology. Note that the viscosity ratio, η_{int}/η_{ext}, plays no role in the steady state reached by the capsule in the tube since the membrane shape is then fixed and the inner liquid is in solid translation.

The characteristics of the outer flow, which could be accurately adjusted by the experimental set-up described in § 3, are very close to the ideal model. In particular, we checked that the pressure drop was in agreement with the Poiseuille law and we investigated a velocity range ($1 \leqslant U \leqslant 34\,\mathrm{mm\,s^{-1}}$) that ensures that the Reynolds number, $Re = 2UR\rho_{ext}/\eta_{ext}$, was always less than 0.15. However, on the other hand, we saw in § 2 that real capsules differ somewhat from the ideal model in two ways. First, the density of the inner fluid is slightly larger than that of the outer fluid, $(\rho_{int} - \rho_{ext})/\rho_{int} \approx 0.03$, so the capsule sediments in a fluid at rest. Secondly, we also saw that the capsules are not perfectly spherical. Their initial state can thus be characterized by the radius, a, of the sphere which has the same volume and the ratio, S, between their minimum to maximum lengths ($0.86 \leqslant S \leqslant 0.95$). Since these two imperfections are expected to alter the flow axisymmetry, we have tried to estimate their importance by performing a series of preliminary tests where two perpendicular views of the capsule steady shape, one horizontal and the other vertical, were taken.

We first investigate the role of buoyancy by considering the location of the capsule centre. Figure 3 shows the transverse horizontal coordinate, y_g, and the vertical

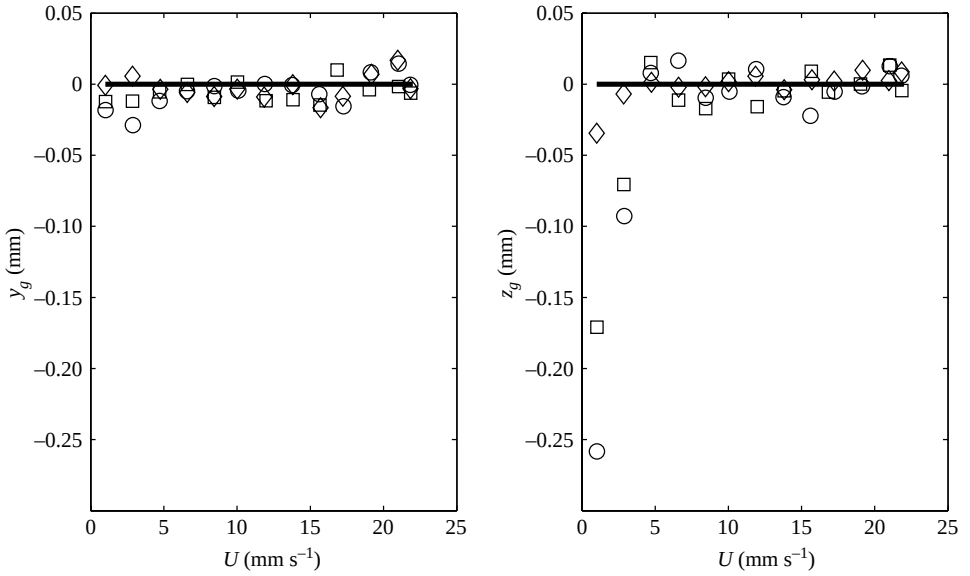

FIGURE 3. Horizontal and vertical locations of the centre of three different capsules as a function of the bulk fluid velocity: ○, $a/R = 0.75$; □, $a/R = 0.80$; ◇, $a/R = 0.87$.

coordinate, z_g, of the centre of three different capsules which have the same elastic modulus, but different sizes. The origin is located on the tube axis so that y_g and z_g measure the capsule off-centring. It is observed that all capsules are centred in the horizontal direction whatever the flow rate is. This is due to the lubrication force exerted on the capsule by the thin liquid film around the capsule between the membrane and the tube wall. Since this hydrodynamic force increases as the film becomes thinner, the stable position of the capsule centre is on the tube axis in absence of buoyancy. In the vertical direction, we observe that at low velocity the capsule centre is under the tube axis. Since the hydrodynamic force is an increasing function of U, the off-centring is observed to decrease as the flow rate is increased. On the other hand, when the size ratio a/R increases, the capsule volume increases and the film thickness decreases, therefore both the hydrodynamic force and the buoyancy increase. However, the hydrodynamic force increases more quickly than the buoyancy, so the capsule centring is achieved sooner for large capsules than for small ones. A complete investigation of the role of buoyancy at low flow velocities would require us also to take into account the capsule deformability characterized by its elastic moduli. This is beyond the scope of the present work. From these preliminary tests, it was possible to conclude that the vertical off-centring was negligible as soon as the velocity was larger than $5\,\mathrm{mm\,s^{-1}}$. In the next section, we will present only results for which the effect of buoyancy is negligible.

We now focus on the effect of the slight non-sphericity of the initial shape. Since the capsules are slightly over-inflated, the existence of an initial departure from sphericity implies that the capsule presents either an anisotropic tension in the membrane at rest or mechanical properties that are non-uniform over the membrane. To check the importance of this initial anisotropy, let us consider the maximal lengths of the capsules in axial, L_x, lateral, L_y, and vertical, L_z, directions. Figure 4 presents the evolution of the maximal lengths against the liquid velocity for two capsules which have one of the worst sphericity ratios ($S = 0.89$). Figure 4(a) shows the results

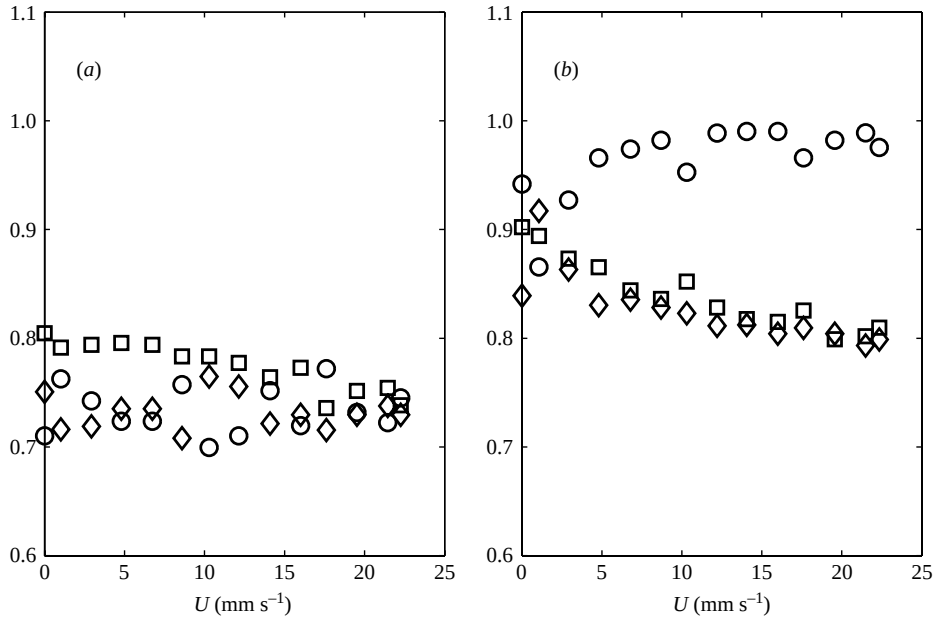

FIGURE 4. Maximal dimensions of two capsules, (*a*) $a/R = 0.75$ and (*b*) $a/R = 0.87$: ○, $L_x/2R$; □, $L_y/2R$; ◇, $L_z/2R$.

corresponding to the smallest capsule ($a/R = 0.75$). Note that the initial orientation of the capsule at the tube entry is not under our control and appears to be random. However, we observe that at low velocity the largest dimension is always the horizontal transverse direction (L_y). The smallest and the medium dimensions may be either L_x or L_z depending on the initial orientation of the capsule. When the velocity increases, the hydrodynamic forces in the film surrounding the membrane increase and tend to make the capsule shape axisymmetric. Above a critical velocity, the deformation of the membrane that is driven by the hydrodynamic stress overcomes the initial anisotropic tensions (or the non-homogeneity of the elastic moduli) that are responsible for the initial non-sphericity and then $L_y = L_z$. This critical velocity is about $15\,\mathrm{mm\,s^{-1}}$ for the small capsule presented in figure 4(*a*), but less than $1.5\,\mathrm{mm\,s^{-1}}$ for the larger capsule presented in figure 4(*b*). As for the problem of capsule centring, we observe that larger the capsule is, the sooner hydrodynamic stresses dominate and the sooner capsule imperfections can be neglected. The different tests we have carried out showed that the effect of the initial disparity in sphericity could always be neglected as soon as the axial length had become the largest one. Beyond this limit, no difference was observed between the different capsules or for the different initial orientations of a given capsule; in particular, the buckling transition that occurred at the capsule rear was not influenced by the initial anisotropy. In the next section, we will present only results obtained in the horizontal plane (x,y). For a/R larger than 0.8 or capillary number Ca larger than 0.015, the results are representative of the ideal situation of initial spherical capsules. (For $a/R = 0.75$ and $Ca \leqslant 0.015$, the measured transversal length L_y might be larger than the radial length of a perfectly spherical capsule of about $(1 - S)/2 \approx 5\,\%$.

Another problem with the capsules is that we did not obtain a complete characterization of the properties of their membrane. Only nine of the 28 capsules used in the present flow experiments have been submitted to compression tests. Moreover, if

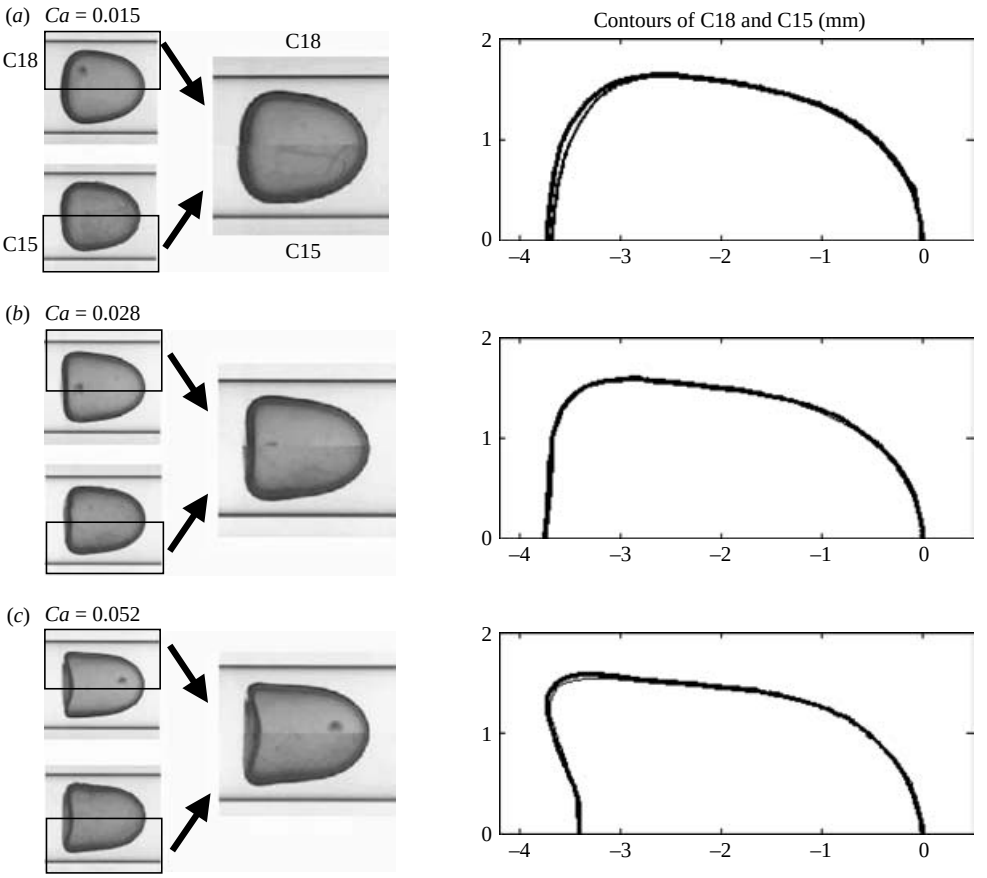

FIGURE 5. Shape comparisons of two capsules C18 and C15 which have the same size ($a/R = 0.83$). C18: $K = 0.30\,\mathrm{N m^{-1}}$; (*a*) $U = 4.7\,\mathrm{mm\,s^{-1}}$, (*b*) $U = 8.5\,\mathrm{mm\,s^{-1}}$, (*c*) $U = 15.5\,\mathrm{mm\,s^{-1}}$; C15: $K = 0.55\,\mathrm{N m^{-1}}$; (*a*) $U = 8.4\,\mathrm{mm\,s^{-1}}$, (*b*) $U = 15.5\,\mathrm{mm\,s^{-1}}$, (*c*) $U = 28.9\,\mathrm{mm\,s^{-1}}$.

compression tests provided a fairly accurate determination of the elastic dilation modulus K, they only led to the conclusion that the shear elastic modulus μ lay between $K/3$ and K. We first checked that the present results were consistent with compression experiments by considering the capsules which had a known elastic modulus. Figure 5 compares the images and contours of two capsules which have the same size, but different K. The liquid velocity has been adjusted in order to obtain the same capillary numbers, $Ca = \eta_{ext} U/K$, for the two capsules. Figure 5 shows that the shapes of the two capsules match very well. Similar comparisons between the other capsules of known K confirmed that the results were the same provided that Ca and a/R were the same. If there were any differences in the value of μ, their effect was not significant. Therefore, the present experiments could be used to characterize the capsules that had not been subjected to compression tests. Their area dilation modulus was determined as follows. We chose a reference capsule whose size was the same as the test capsule whose dilation elastic modulus K had to be measured. Of course, the reference capsule could not have exactly the same size as the test capsule, but the maximal difference was less than 2.5 % and comparisons with different capsules of close sizes allow us to minimize the error introduced by small size differences. Now, let us denote the liquid velocity corresponding to the reference capsule as U_{ref} and that

of the test capsule as U_{test}. For a given U_{ref}, we searched the value of U_{test} for which the shape of the test capsule matched that of the reference capsule. Then, we deduced the value of K of the test capsule by equating its capillary number with that of the reference capsule. This method was applied to each velocity U_{ref} for which there was a velocity U_{test} allowing the contour matching. Finally, we retained the value of K that provided the best agreement over all available velocity pairs. Note that each time an elastic modulus had been determined, the corresponding capsule could be used as a reference capsule. Thus at the end of the process, many comparisons could be made, allowing a reliable validation of this method which appeared to be at least as accurate as the compression method ($\pm 5\,\%$).

5. Experimental results

We analyse now the steady states reached by the capsules that flow in the narrow tube and focus on the effects of the capillary number and size ratio. Figure 6 shows top-view pictures of the capsules. We selected four size ratios ($a/R = 0.75$, 0.81, 0.87 and 0.94) and various capillary numbers covering the range investigated. The contours corresponding to each size ratio have been superimposed in figure 7 by using the capsule front as the origin of coordinates. The evolution of the capsule shape with the capillary number is qualitatively the same for all size ratios. When Ca is increased, the capsule extends in the axial direction and contracts in the radial one. To describe this process in detail, it is useful to distinguish the front, the rear and the intermediate parts of the capsule. During a first stage, the curvature of the front increases and the intermediate part lengthens. When increasing Ca further, both the front and intermediate parts stop evolving. Concerning the capsule rear, initially convex, it first flattens, becomes concave and then becomes more and more concave as Ca is increased.

These observations suggest that we should introduce the following parameters for characterizing the capsule shape: the maximal axial dimension, L_x, and the maximal lateral one, L_y, the distance L_{fr} between the front and the rear measured on the axis of symmetry, the curvature C_f of the front and that of the rear, C_r (see figure 8). In order to characterize the membrane deformation, it is also useful to measure the two principal extension ratios of the membrane, in the meridian direction, λ_m, and in azimuthal one, λ_ϕ. It is not possible to determine their local values since we do not know the Lagrangian coordinates of each membrane point. We thus introduce the following global values: $\langle\lambda_m\rangle$ is the ratio of the measured contour perimeter with the perimeter of a circle of radius a; $\langle\lambda_\phi\rangle = (1 + \langle\alpha\rangle)/\langle\lambda_m\rangle$ where $\langle\alpha\rangle$ is the area variation of the membrane relative to its shape at rest.

Figure 9 presents the evolution of all these parameters against the capillary number for $a/R = 0.81$. Figure 9(a) shows that the axial length L_x is an increasing function of Ca, which confirms that the larger is the viscous stress, the more stretched is the capsule. Nevertheless, this general mechanism involves two different stages. As long as the curvature of the rear remains positive ($Ca \leqslant 0.03$), the capsule becomes narrower and the curvature of its front increases. The conservation of the capsule volume is thus ensured by the decrease of L_y that compensates for the increase of L_x. After the formation of the concave part at the rear of the capsule ($Ca > 0.03$), L_x goes on increasing but L_y and the front curvature have reached constant values. On the other hand, the distance between the capsule front and the capsule rear, L_{fr}, is then a decreasing function of Ca. During this second stage, the volume conservation is then ensured by the concave part at the capsule rear becoming deeper and deeper.

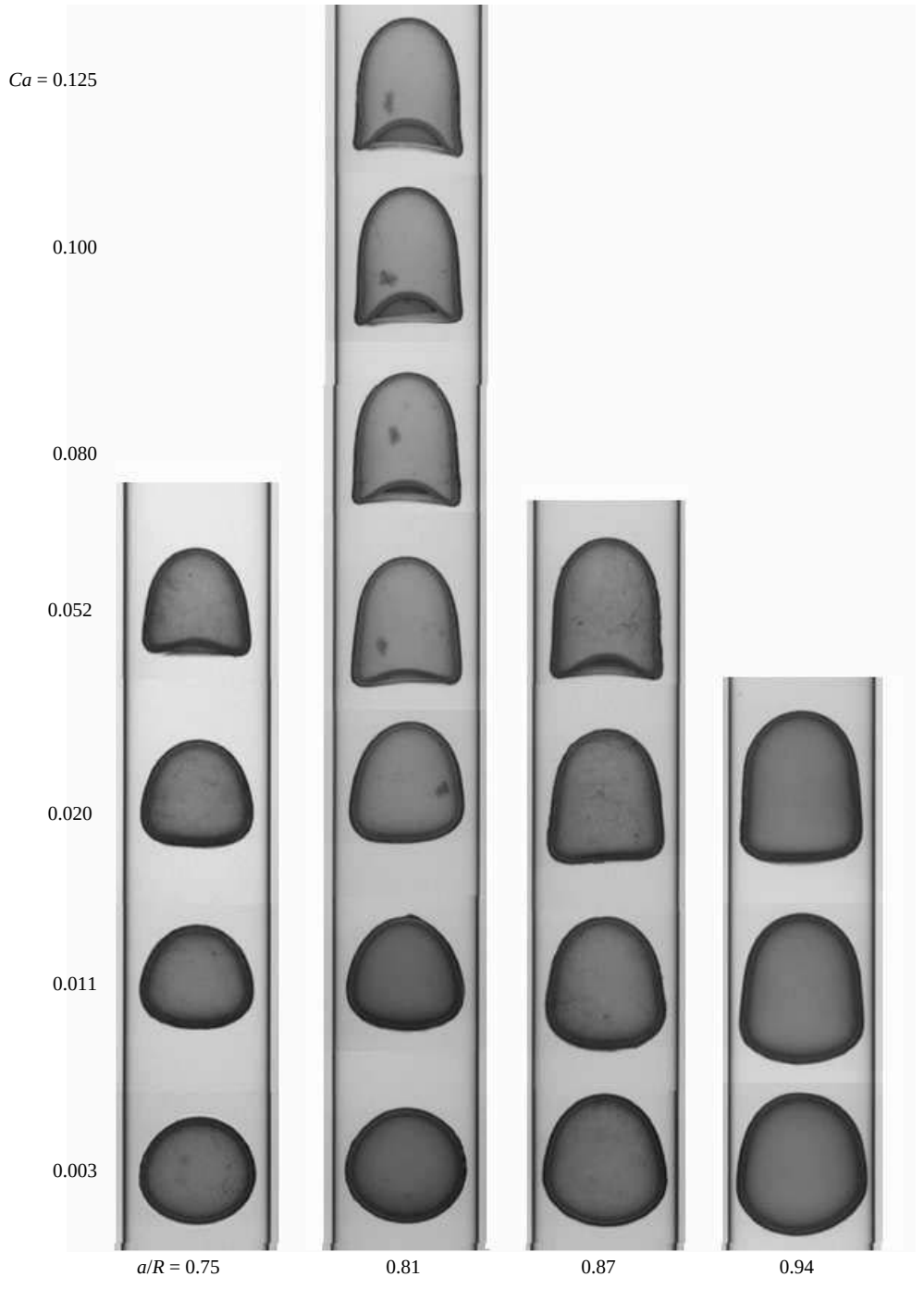

FIGURE 6. Stationary shapes for different capillary numbers and a/R: $a/R = 0.75$ capsules C22 ($Ca = 0.003$) and C13 ($Ca = 0.011$–0.052); $a/R = 0.81$ capsules C2 ($Ca = 0.003$–0.0011) and C17 ($Ca = 0.020$–0.125); $a/R = 0.87$ capsules C27 ($Ca = 0.003$) and C12 ($Ca = 0.011$–0.052); $a/R = 0.94$ capsule C6.

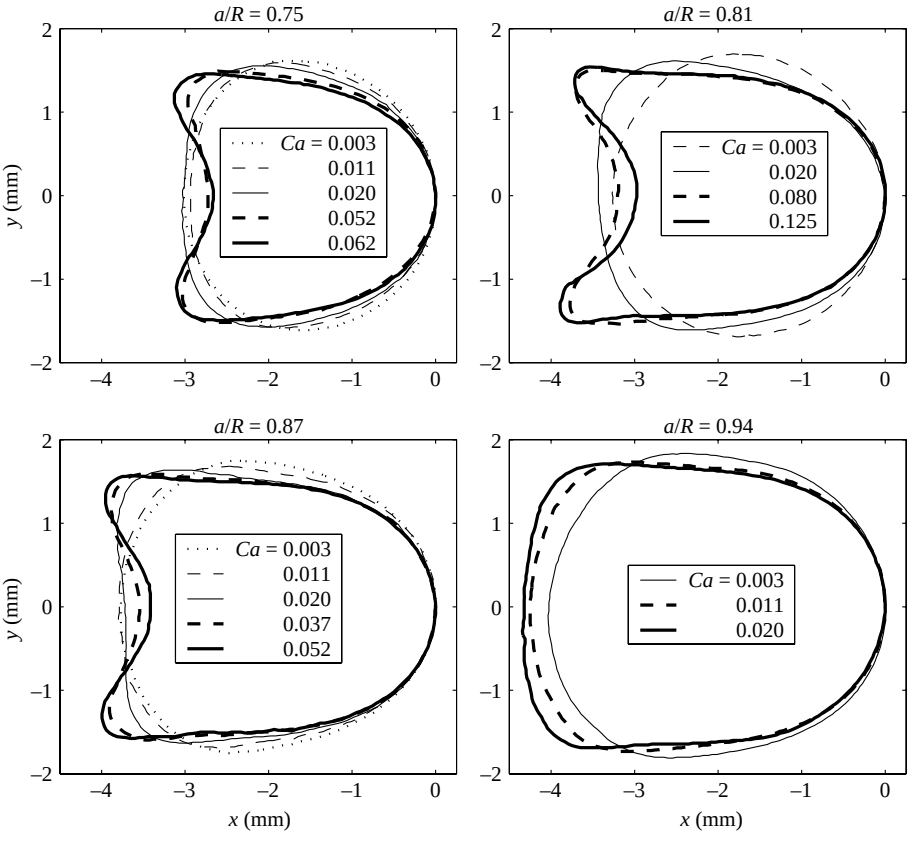

FIGURE 7. Stationary contours for different capillary numbers and a/R: same capsules as in figure 6.

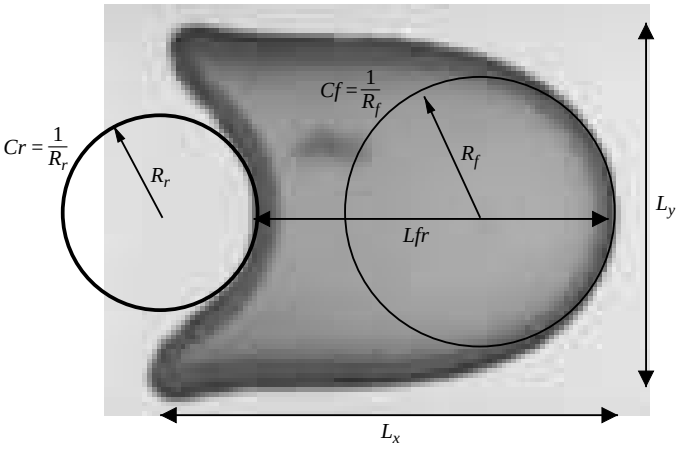

FIGURE 8. Definition of parameters for shape characterization.

Owing to the axisymmetry, the volume conservation requires that the decrease in length close to the axis, L_{fr}, be much larger than the increase in length close to the tube wall, L_x. This particular process of deformation implies that the membrane extension ratio in the azimuthal direction remains close to unity although the capsule

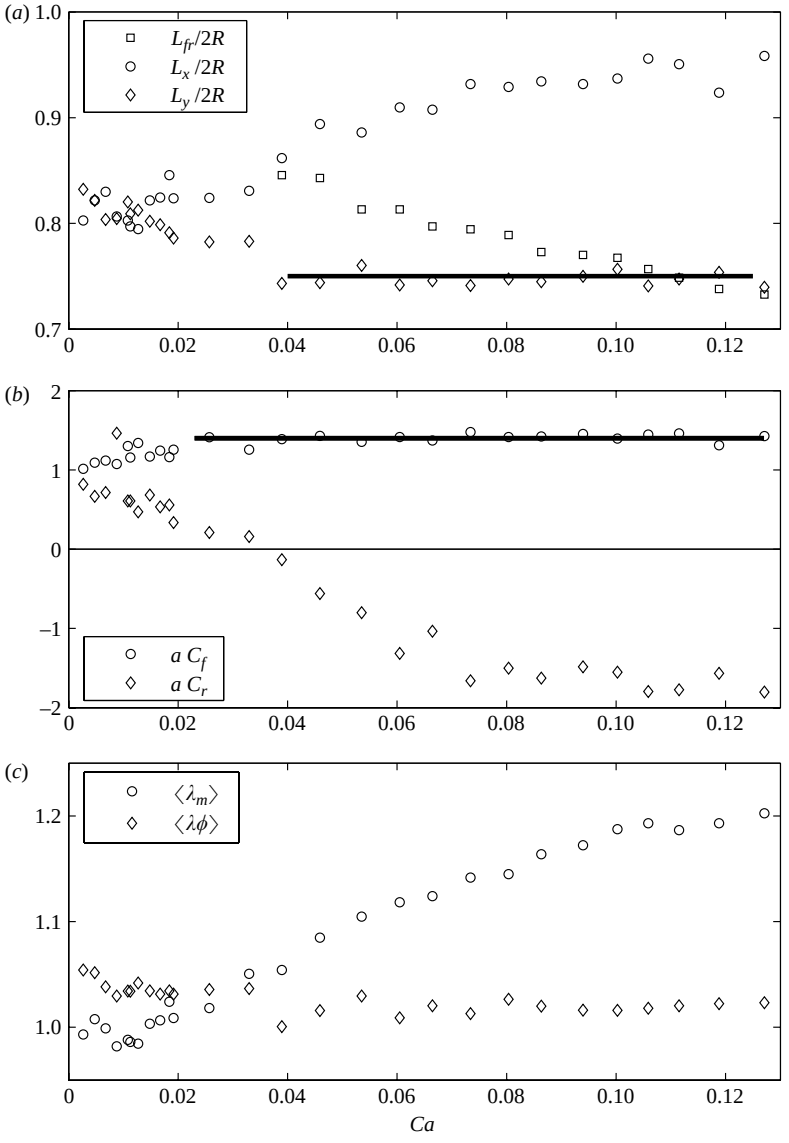

FIGURE 9. Evolution of the capsule shape as a function of Ca for $a/R = 0.81$: (a) axial and lateral dimensions; (b) front and rear curvatures; (c) global extension ratios.

is significantly stretched in the meridian direction (figure 9c). Moreover, it also implies that the increase of $\langle\lambda_m\rangle$ with Ca, and so that of the membrane tensions, is more rapid than the increase of L_x. Finally, we observed that the curvature of the rear reaches a constant value around $Ca = 0.08$ and the deformation seems to slow down afterwards.

The process of deformation is similar for all the capsule sizes investigated ($0.75 \leqslant a/R \leqslant 0.95$). In each case, L_y and C_f reach constant final values when Ca becomes large enough. Figure 10 shows the evolution of the final constant values of the lateral dimensions $L_y^{lim}/2a$ and of the front radius of curvature R_f^{lim}/a against a/R. Note that

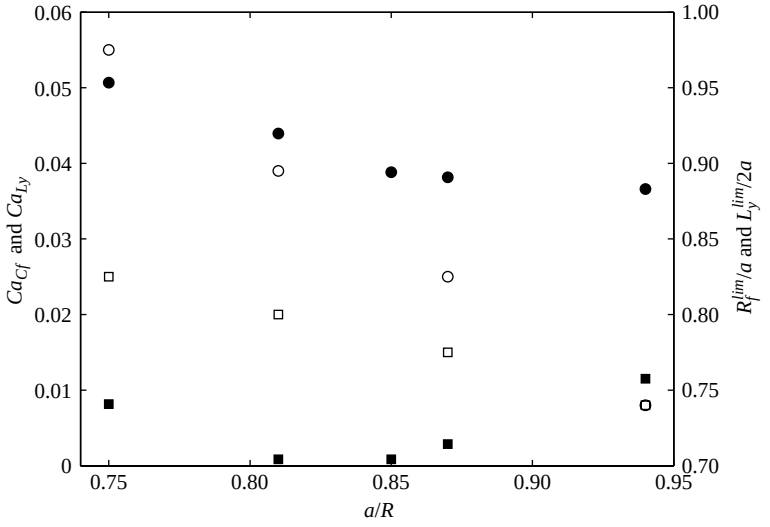

FIGURE 10. Asymptotic behaviour at large Ca. Left axis: □, Ca_{Cf}; ○, Ca_{Ly}. Right axis: ■, R_f^{lim}/a; ●, $L_y^{lim}/2a$.

both have been normalized by the initial capsule radius. When it is not normalized, $L_y^{lim}/2$ (resp. R_f^{lim}) regularly increases from $0.71R$ to $0.83R$ (resp. from $0.56R$ to $0.71R$) when a/R is increased from 0.75 to 0.94. Hence, the width of the gap between the membrane and the wall decreases, and so lubrication force increases, when the capsule becomes larger. When normalized by a, the final lateral dimension is a decreasing function of a/R, whereas the radius of curvature of the front becomes almost independent of a/R, its value lying in the range 0.70–0.75. This indicates that even if the overall departure from the initial spherical shape increases with a/R, the deformation of the very front part tends toward an asymptotic state independent of both Ca and a/R. Figure 10 also presents the capillary numbers, Ca_{Ly} and Ca_{Cf}, for which $L_y^{lim}/2$ and R_f^{lim} are reached. The larger a/R is, the smaller Ca_{L_y} and Ca_{C_f} are. Even if the deformation process is similar whatever a/R, its successive stages happen for lower values of Ca when a/R becomes larger.

Figure 11 shows the global extension $\langle\lambda_m\rangle$ against the capsule size a/R for three different capillary numbers. Here, we show only the meridian extension ratio since the azimuthal one remains close to unity in each case. Note that for all the tests performed in the present study, $\langle\lambda_m\rangle$ did not exceed 1.2 and the relative membrane area variation did not exceed 0.23. We checked that the membrane material always remained in the elastic domain, as could be expected from the results of the compression experiments. In this regime, we observed that the membrane extension is an increasing function of both a/R and Ca.

We now analyse the velocity V of the capsule. Figure 12 shows the relative velocity difference, $V/U - 1$, against the capillary number for different capsule sizes. Note that even for a given value of a/R, each plot collects the results from several different capsules. The fact that the evolutions of the capsule velocity against Ca lie on reasonably smooth curves confirms that Ca and a/R are the only significant control parameters for the present experiments. In all cases, the capsule velocity is larger than the bulk fluid velocity U, but less than the maximal liquid velocity on the axis

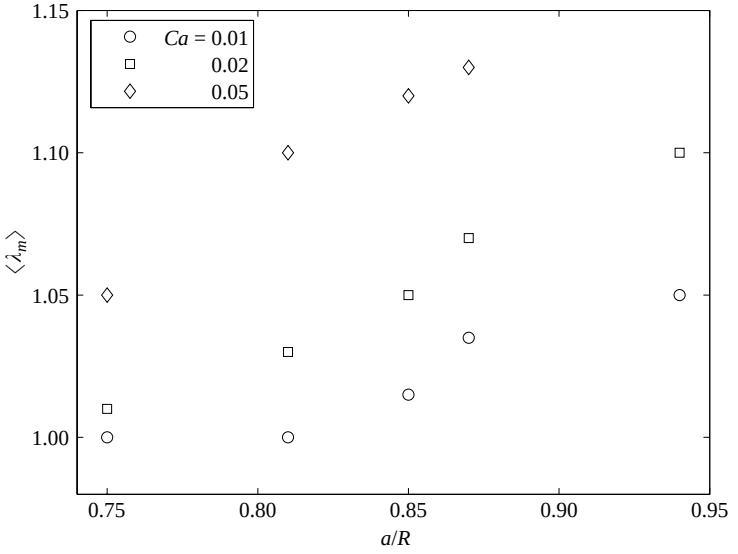

FIGURE 11. Global meridian extension ratio against a/R: ○, $Ca = 0.01$; □, $Ca = 0.02$; ◇, $Ca = 0.05$.

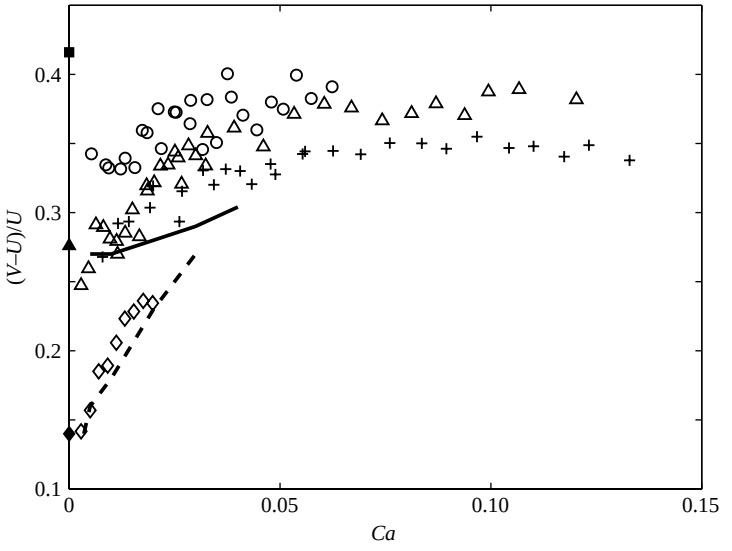

FIGURE 12. Capsule velocity relative to the bulk liquid velocity. Experiments: ○, $a/R = 0.75$; △, $a/R = 0.81$; +, $a/R = 0.85$; ◇, $a/R = 0.94$. Numerical simulations by Quéguiner & Barthès-Biesel (1997): —, $a/R = 0.80$; – – –, $a/R = 0.90$. Theory for a rigid spheres by Wang & Skalak (1969): ■, $a/R = 0.70$; ▲, $a/R = 0.80$; ◆, $a/R = 0.90$.

$2U$. The thinner the gap between the membrane and the tube wall is, the slower the capsule flows, its velocity decreasing towards the bulk liquid velocity. The evolution of capsule velocity can consequently be qualitatively predicted from what we know about the capsule deformation. From the observed evolution of L_y, we may indeed anticipate that $V/U - 1$ is a increasing function of Ca that tends towards a constant

value at large capillary numbers and is a decreasing function of a/R. The asymptotic values of the capsule velocity have only been attained for certain capsule sizes: $(V/U-1)_{lim}=0.38$ for $a/R=0.81$ and $(V/U-1)_{lim}=0.35$ for $a/R=0.85$. Figure 12 also shows the numerical results obtained by Wang & Skalak (1969) for rigid spheres in creeping flow as reference cases for $Ca=0$ and those obtained for capsules by Quéguiner & Barthès-Biesel (1997), which will be commented on in the next section.

6. Discussion

We investigated experimentally the behaviour of initially spherical capsules flowing in a narrow tube ($0.75 \leqslant a/R \leqslant 0.95$) at low to moderate capillary numbers ($Ca \leqslant 0.125$) and observed the following general trends. At low Ca, the capsule is rounded at both ends. When Ca increases, its length increases, its radial dimension decreases and its rear flattens. Beyond a certain Ca, the capsule rear becomes concave. Increasing Ca further, the capsule length still increases and the negative curvature of the rear goes on decreasing, but its radial dimension reaches a constant value.

In order to determine to what extent the results are specific to the membrane rheology of the present capsules, we can compare them with other experimental results obtained with different kinds of capsules. First, consider the case of droplets. Note that droplets can be considered as capsules which have a particular membrane rheology, i.e. with isotropic tensions independent of the deformation. There are many works dealing with droplets flowing in a narrow tube ($a/R > 0.7$) at low Reynolds number. We will refer here to the major contributions by Ho & Leal (1975) and Olbricht & Kung (1992). For droplets, the results do not depend only on the capillary number and the size ratio, but also on the viscosity ratio. For any fixed η_{int}/η_{ext}, the qualitative behaviour at low Ca is similar to what we observed with capsules: a rounded shape at both ends with a rear that flattens and a length that increases with increasing Ca. In each case, there exists a critical capillary number, larger than unity, beyond which breakup occurs. At low η_{int}/η_{ext}, the rear of the droplet becomes concave and a finger of the outer liquid penetrates the droplets which eventually break up. At large η_{int}/η_{ext}, the droplet is stretched in the axial direction until it ruptures, the penetration of a finger of outer liquid from the rear also occurs simultaneously in some cases. Vitkova *et al.* (2004) investigated lipid vesicles with diameters in the range 10–70 μm flowing through capillaries. The size ratio a/R was in the range 0.2–1.1 and the viscosity ratio η_{int}/η_{ext} was close to unity. When increasing the liquid velocity, the vesicle length and its front curvature increase, whereas the rear curvature decreases. For large flowing velocities, concave rears were also observed. Lee & Fung (1969) carried out the experimental study of flexible thin-walled rubber cells, liquid-filled and geometrically similar to red blood cells. The cells were flowing in a very viscous silicone oil in order to ensure small Reynolds numbers, despite a cell diameter larger than 4 cm. The ratio between the cell equatorial radius and that of the tube was in the range 0.98–1.7. Contrary to droplets and lipid vesicles, these cells were macroscopic objects with a membrane made of a thin layer of a three-dimensional material. We may thus expect a membrane rheology closer to the capsules used here. On the other hand, the initial biconcave shape constitutes an important difference. The cell was observed to flow sideways with its equatorial plane parallel to the tube axis. For $a/R=0.98$, the cell remained biconcave only at very low velocity. When the velocity becomes large enough, the membrane buckles either at its trailing edge or symmetrically with the leading pole moving away from the centre while the trailing

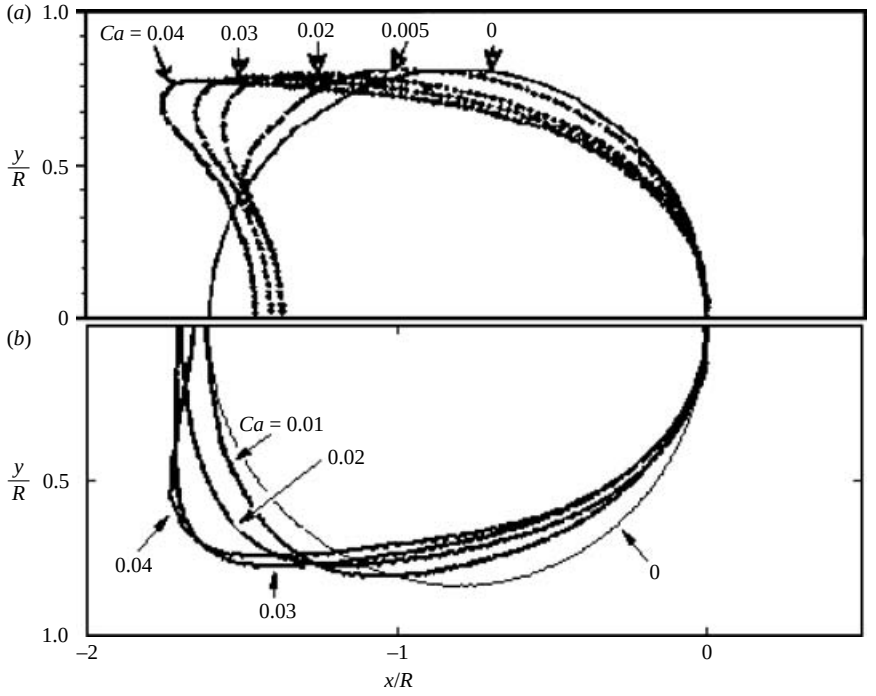

FIGURE 13. Comparison between experiments and the numerical simulations for $a/R = 0.80$. (*a*) Simulation by Quéguiner & Barthès-Biesel (1997) for a Mooney–Rivlin membrane; (*b*) present experiments with capsule C16.

pole moves toward the centre. Whatever a/R, the cell buckled at large velocity, the trailing end always buckling inward.

After the pioneering works of Barnard, Lopez & Hellums (1968) and Lighthill (1968), there were several attempts based on lubrication theory to address the problem of the flow of red blood cells along narrow vessels. The work of Secomb *et al.* (1986) is particularly interesting. They assumed axisymmetric shapes and used lubrication theory to describe the liquid flow in the gap between the cell and the wall. They investigated situations with only isotropic membrane tensions and then considered the effects of shear and bending. They predicted shapes with rounded front and concave rear in qualitative agreement with those observed experimentally. The fact that the membrane tension becomes small and even negative in the tail region explained why concave rears are observed. Moreover, the authors remarked that in the absence of bending resistance near the rear, the axisymmetric shape was potentially unstable and might buckle. Quéguiner & Barthès-Biesel (1997) used a boundary integral method to solve numerically the axisymmetric motion and deformation of capsules through cylindrical channels. Figure 13 compares our experimental results with their numerical simulations for $a/R = 0.8$. Note that the simulations considered a Neo-Hookean membrane (NH) with negligible bending stiffness. The NH constitutive law is the simplest version of the Mooney–Rivlin (MR) law and is defined by (2.4) where $\Psi' = 0$. The NH model hence involves a unique parameter, the surface shear modulus G^{MR}, or equivalently the Young's modulus $Es = 3G^{MR}$. The capillary number used by Quéguiner & Barthès-Biesel (1997) was $Ca = \eta_{ext} U/Es$. Since $K_0 = 3G^{MR} = Es$,

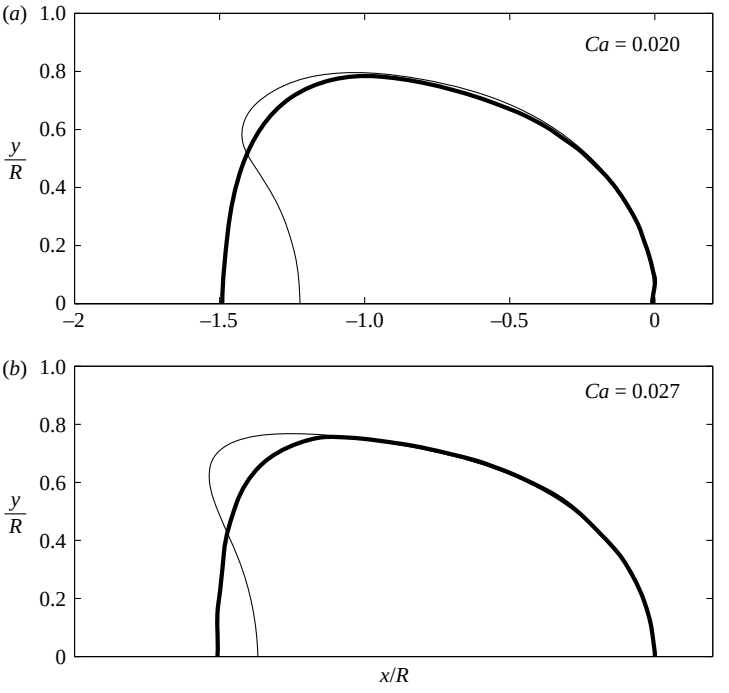

FIGURE 14. Comparison between experiments and numerical simulations for $a/R = 0.78$. Thin lines: simulations by Diaz & Barthès-Biesel (2001) for a (ES) membrane with (*a*) $\mu/K = 1$ or (*b*) $\mu/K = 1/3$. Thick lines: present experiments with capsule C28.

the experimental and numerical capillary numbers are the same and the results can be compared directly. (See Barthès-Biesel, Diaz & Dhenin, 2002, for a thorough discussion of how results obtained with different constitutive laws can be compared). Figure 13 shows that if the order of magnitude of the overall deformation is comparable, the shapes are significantly different. In particular, we observe that the concave part at the capsule rear is deeper and occurs for a smaller value of Ca in the simulations than in the experiments. As can be seen in figure 12, these different shapes induced differences in the capsule velocity. If, at low Ca, experimental and numerical results are both close to the theoretical solution obtained by Wang & Skalak (1969) for a solid sphere, they diverge from each other at large Ca. These differences could be expected since the NH law is not valid for the description of the membrane of the present capsules. Diaz & Barthès-Biesel (personal communication 2001) performed additional numerical simulations by assuming a membrane material with constant elastic moduli (ES model). They kindly provided us with some calculated shapes for $a/R = 0.78$. Comparisons with experiments were possible for three cases: $Ca = 0.016$ for $\mu/K = 1/10$, $Ca = 0.027$ for $\mu/K = 1/3$ and $Ca = 0.020$ for $\mu/K = 1$. For $\mu/K = 1/10$, both the front and the rear parts of the calculated shapes differ from the experimental ones. On the other hand, figure 14 shows that the shapes calculated for $\mu/K = 1/3$ and 1 matched well the experimental ones at the front and intermediate parts, but not at the rear where they predicted deeper concave parts. These results suggest that either the bending stiffness or the initial capsule inflation may play a crucial role in the behaviour of the capsule rear. First, it is worth recalling

that small, but non-zero, bending moments are necessary to guarantee the stability of the observed shapes. In the simulation of Quéguiner & Barthès-Biesel (1997) who assumed zero bending stiffness, the calculated shape was smoothed at each time step in order to ensure the stability of the computation. Diaz & Barthès-Biesel (2002) obtained the same results by considering a very weak bending stiffness. Then, Lac *et al.* (2004) investigated numerically different three-dimensional unbounded flows for various membrane laws with negligible bending resistance. They showed that buckling instablity occurs each time there are negative membrane tensions. In the present experiments, this buckling instability did not occur. However, small existing bending moments do not necessarily influence the capsule shape significantly. By assuming that the two-dimensional description of the membrane is obtained by integration of the three-dimensional stresses over the membrane cross-section, the magnitude, ϵ, of the ratio between bending and membrane expansion effects is given by:

$$\epsilon = \frac{h^2 C^2}{\alpha}, \tag{6.1}$$

where h, C and α are, respectively, the membrane thickness, curvature and relative area dilation. Using the maximal curvature, which is observed at the trailing edge of the capsule, and the average area dilation $\langle\alpha\rangle$, we find that ϵ was always less than 2.5 %. This may suggest that membrane bending stiffness probably does not play a significant role in the global shape of the capsule. Nevertheless, we cannot be sure that it is true everywhere since tensions may vanish at the capsule rear. Since the local deformations are unknown, the fact that the global ratio between bending and membrane expansion effects is small has to be considered with caution.

On the other hand, the existence of initial positive tensions may delay the occurrence of negative tensions and thus also prevents membrane buckling. Numerical simulations of a capsule with an STZC membrane (Lefebvre & Barthès-Biesel 2005) indeed show that negative curvatures at the capsule rear are reduced when initial inflation is taken into account. We know from Sherwood *et al.* (2003) that the present capsules are initially slightly over-inflated. For all the results presented here, the initial isotropic inflation, λ_i, was approximately 1.045. To check the influence of this parameter we carried out some additional tests with capsules which were previously immersed in solutions of different salt concentrations. Figure 15 compares the front and rear curvatures for three capsules of the same size ($a/R = 0.75$), but with different initial inflations ($\lambda_i = 1.025$, 1.045 and 1.075). It is remarkable that the measured front curvatures are independent of the initial inflation over the whole range of Ca investigated. On the other hand, the rear curvature is also independent of λ_i up to $Ca = 0.025$ where concave parts start to be observed at the capsule rear. Note that the adjustment of the initial inflation required several additional manipulations during which we did not manage to avoid totally the deposition of a few dust particles on the membrane. If that does not disturb the detection of the convex parts of the capsule contour, this complicates the detection of concave ones (see § 3 and figure 2). For that reason, the negative measured curvatures are not accurate enough to allow a reliable comparison between the three cases.

We presented here an extensive experimental investigation of the steady state of a capsule flowing in a narrow tube in the Stokes regime. The experimental model is representative of an initially slightly over-inflated spherical capsule which is made of a Newtonian drop surrounded by a two-dimensional elastic membrane with constant elastic moduli. The general trends are in qualitative agreement with those observed

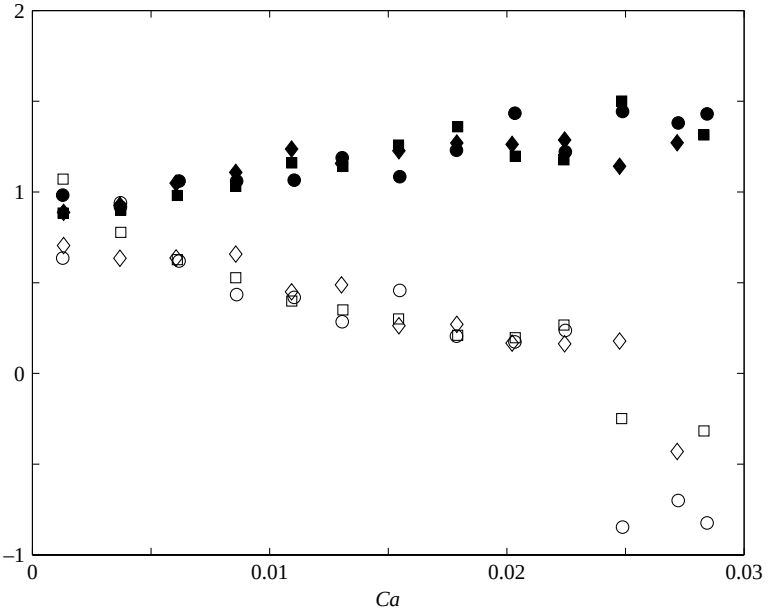

FIGURE 15. Front and rear curvatures against the capillary number for three capsules having the same size ($a/R = 0.75$), but different initial inflation: ○, aC_r and ●, aC_f for $\lambda_i = 1.025$; □, aC_r and ■, aC_f for $\lambda_i = 1.045$; ◇, aC_r and ◆, aC_f for $\lambda_i = 1.075$.

experimentally with similar objects as droplet or lipid vesicles, or numerically with capsules. The prediction of numerical simulations, however, differ quantitatively from the experiments since either a different membrane two-dimensional mechanical law was used or the initial pre-inflation was not considered. The results seem to show that if the membrane rheology controls the whole capsule shape, the initial over-inflation mainly influences the capsule rear. Additional numerical simulations taking into account the initial inflation are now necessary to understand the mechanisms that control the capsule rear and make the capsule width reach an asymptotic value at large capillary number.

We are grateful to thank Florence Edwards-Lévy and Marie-Christine Lévy from the Faculté de Pharmacie De Reims for supplying us with the capsules. We would also like to thank Anna Diaz and Dominique Barthès-Biesel from the Université de Technologie de Compiègne for having provided us with some original numerical simulations.

REFERENCES

BARNARD, A. C. L., LOPEZ, L. & HELLUMS, J. D. 1968 Basic theory of blood flow in capillaries. *Microvasc. Res.* **1**, 23–34.

BARTHÈS-BIESEL, D. 1980 Motion of a spherical microcapsule freely suspended in a linear shear flow. *J. Fluid Mech.* **100**, 831–853.

BARTHÈS-BIESEL, D., DIAZ, A. & DHENIN, E. 2002 Effect of constitutive laws for two-dimensional membranes on flow-induced capsule deformation. *J. Fluid Mech.* **460**, 211–222.

CARIN, M., BARTHÈS-BIESEL, D., EDWARDS-LÉVY, F., POSTEL, C. & ANDREI, D. C. 2003 Compression of biocompatible liquid filled HSA-alginate capsules: determination of the membrane mechanical properties. *Biotechnol. & Bioengng* **82**, 207–212.

Chang, K. S. & Olbricht, W. L. 1993*a* Experimental studies of the deformation of a synthetic capsule in extensional flow. *J. Fluid Mech.* **250**, 587–608.

Chang, K. S. & Olbricht, W. L. 1993*b* Experimental studies of the deformation and break-up of a synthetic capsule in steady and unsteady simple shear flow. *J. Fluid Mech.* **250**, 609–633.

Diaz, A. 2001 Comportement transitoire d'une capsule axisymétrique en suspension. PhD thesis, Université de Technologie de Compiègne.

Diaz, A. & Barthès-Biesel, D. 2002 Entrance of a bioartificial capsule in a pore. *Comput. Mod. Engng Sci.* **3**, 321–337.

Diaz, A., Pelekasis, N. & Barthès-Biesel, D. 2000 Transient response of a capsule subjected to varying flow conditions: effect of internal fluid viscosity and membrane elasticity. *Phys. Fluids* **12**, 948–957.

Discher, B. M., Bermudez, H., Hammer, D. A. & Disher, D. E. 2002 Cross-linked polymersome membranes: vesicles with broadly adjustable properties. *J. Phys. Chem.* B **106**, 2848–2854.

Edwards-Lévy, F. & Lévy, M.-C. 1999 Serum albumin-alginate coated beads: mechanical properties and stability. *Biomaterials* **20**, 2069–2084.

Evans, E. A. & Skalak, R. 1980 *Mechanics and Thermodynamics of Biomembranes*. CRC Press.

Ho, B. P. & Leal, L. G. 1975 The creeping motion of liquid drops through a circular tube of comparable diameter. *J. Fluid Mech.* **71**, 361–383.

Joly, A., Desjardins, J.-F., Fremond, B., Desille, M., Campion, J.-P., Malledant, Y., Lebreton, Y., Semana, G., Edwards-Lévy, F., Lévy, M.-C. & Clément, B. 1997 Survival, proliferation, and functions of porcine hepatocytes encapsulated in coated alginate beads: a step towards a reliable bioartificial liver. *Transplantation* **63**, 795–803.

Lac, E. & Barthès-Biesel, D., Pelekasis, N. A. & Tsamopoulos, J. 2004 Spherical capsules in three-dimensional unbounded Stokes flows: effect of the membrane constitutive law and onset of buckling. *J. Fluid Mech.* **516**, 303–334.

Lee, J. S. & Fung, Y. C. 1969 Modeling experiments of a single red blood cell moving in a capillary blood vessel. *Microvasc. Res.* **1**, 221–243.

Lefebvre, Y. & Barthès-Biesel, D. 2005 Effet de la pression osmotique sur l'écoulement de capsules bioartificielles dans un tube. *Proc. 17th Congrès Francais de Mécanique*, Paper 942, CD-ROM.

Lévy, M.-C. & Edwards-Lévy, F. 1996 Coating alginate beads with cross-linked biopolymers: a novel method based on a transacylation reaction. *J. Microencapsulation* **13**, 169–183.

Lighthill, M. J. 1968 Pressure-forcing of tightly fitting pellets along fluid-filled elastic tubes. *J. Fluid Mech.* **34**, 113–143.

Mohandas, N. & Evans, E. 1994 Mechanical properties of the red cell membrane in relation to molecular structure and genetic defects. *Annu. Rev. Biophys. Biomol. Struct.* **23**, 787–818.

Olbricht, W. L. & Kung, D. M. 1992 The deformation and breakup of liquid drops in low Reynolds number flow through a capillary. *Phys. Fluids* A **4**, 1347–1354.

Pozrikidis, C. 2001 Effect of membranes bending stiffness on the deformation of capsules in simple shear flow. *J. Fluid Mech.* **440**, 269–291.

Quéguiner, C. & Barthès-Biesel, D. 1997 Axisymmetric motion of capsules through cylindrical channels. *J. Fluid Mech.* **348**, 349–376.

Ramanujan, S. & Pozrikidis, C. 1998 Deformation of liquid capsules enclosed by elastic membranes in simple shear flow: large deformations and the effect of fluid viscosities. *J. Fluid Mech.* **361**, 117–143.

Risso, F. & Carin, M. 2004 Compression of a capsule: mechanical laws of membranes with negligible bending stiffness. *Phys. Rev.* E **69**, 061601

Secomb, T. W., Skalak, R., Özkaya, N. & Gross, J. F. 1986 Flow of axisymmetric red blood cells in narrow capillaries. *J. Fluid Mech.* **163**, 405–423.

Sherwood, J. D., Risso, F., Collé-Paillot, F., Edwards-Lévy, F. & Lévy, M.-C. 2003 Rates of transport through a capsule membrane to attain Donnan equilibrium. *J. Colloid Interface Sci.* **263**, 202–212.

Shinya, E., Dervillez, X., Edwards-Lévy, F., Duret, V., Brisson, E., Ylisastigui, L., Lévy, M.-C., Cohen, J. H. M. & Klatzmann, D. 1999 In-vivo delivery of therapeutic proteins by genetically-modified cells: comparison of organoids and human serum albumin alginate-coated beads. *Biomed. Pharmacotherapy* **53**, 471–483.

Skalak, R., Özkaya, N. & Skalak, T. C. 1989 Biofluid mechanics. *Annu. Rev. Fluid Mech.* **21**, 167–204.

Skalak, R., Tözeren, A., Zarda, R. P. & Chien, S. 1973 Strain energy function of red blood cell membranes. *Biophys. J.* **13**, 245–254.

Smith, A. E., Zhangdagger, Z., Thomas, C. R., Moxham, K. E., Middelberg, A. P. J. 2000 The mechanical properties of Saccharomyces cerevisiae. *Proc. Natl Acad. Sci. USA* **97**, 9871–9874.

Vitkova, V., Mader, M. & Podgorski, T. 2004 Deformation of vesicles flowing through capillaries. *Europhys. Lett.* **68**, 398–404.

Wang, H. & Skalak, R. 1969 Viscous flow in a cylindrical tube containing a line of spherical particles. *J. Fluid Mech.* **38**, 75–96.